Hindawi
Journal of Chemistry
Volume 2019, Article ID 7387234, 13 pages
https://doi.org/10.1155/2019/7387234

*Research Article*

# Numerical Simulation of Shale Gas Multiscale Seepage Mechanism-Coupled Stress Sensitivity

**Xun Yan,[1] Jing Sun,[1] and Dehua Liu[1,2]**

[1]*School of Petroleum Engineering, Yangtze University, Wuhan 434023, Hubei, China*
[2]*Hubei Shale Gas Development Engineering Research Center, Wuhan 434023, Hubei, China*

Correspondence should be addressed to Jing Sun; 77220250@qq.com

Received 26 December 2018; Revised 12 February 2019; Accepted 25 February 2019; Published 25 March 2019

Academic Editor: Dapeng Cao

Copyright © 2019 Xun Yan et al. This is an open access article distributed under the Creative Commons Attribution License, which permits unrestricted use, distribution, and reproduction in any medium, provided the original work is properly cited.

The complexity of the gas transport mechanism in microfractures and nanopores is caused by the feature of multiscale and multiphysics. Figuring out the flow mechanism is of great significance for the efficient development of shale gas. In this paper, an apparent permeability model which covers continue, slip, transition, and molecular flow and geomechanical effect was presented. Additionally, a mathematical model comprising multiscale, geomechanics, and adsorption phenomenon was proposed to characterize gas flow in the shale reservoir. The aim of this paper is to investigate some important impacts in the process of gas transportation, which includes the shale stress sensitivity, adsorption phenomenon, and reservoir porosity. The results reveal that the performance of the multistage fractured horizontal well is strongly influenced by stress sensitivity coefficient. The cumulative gas production will decrease sharply when the shale gas reservoir stress sensitivity coefficient increases. In addition, the adsorption phenomenon has an influence on shale gas seepage and sorption capacity; however, the effect of adsorption is very weak in the early gas transport period, and the impact of later will increase. Moreover, shale porosity also greatly affects the shale gas transportation.

## 1. Introduction

Shale gas is an unconventional energy with extensive distribution and large reserves, which can alleviate the pressure of global natural gas supply and demand gap. Furthermore, it can also provide reliable energy supply for the sustainable development of the world economy. However, the understanding of the shale gas flow mechanism is far behind production practice. Many relevant studies show that the gas transportation exhibits the characteristics of multiscale. In addition, the influence of stress sensitivity on seepage flow cannot be neglected. Therefore, it is very important to understand the multiscale seepage mechanism of shale gas under stress sensitivity.

Many previous works have been performed to understand the characteristics of gas flow and stress sensitivity in shale gas [1–3]. Huang et al. [1] shows that gas transportation in shale cannot be simply characterized by the Darcy law, and a method by calculating the Knudsen number was proposed to analyze the shale gas flow regime. Additionally, a unified model taking into account slip and real gas effect was proposed to model gas transport behavior for different gas transport mechanisms in nanopores [4]. Zhang et al. [5] studied the stress sensitivity characteristics of shale with experiments, and the research results showed that the stress sensitivity of the shale core used in this experiment was generally higher than that of tight sandstone. Meanwhile, the study also pointed out that the compressibility of shale is much higher than that of sandstone due to the strong compressibility of shale nanopores, microfractures, and clay minerals. Besides, the gas flow mechanism of fractured vertical well with stress sensitivity is also studied [6]. However, little work has been done to investigate multiscale gas flow coupling stress sensitivity.

In this paper, a mathematical model comprising multiscale, geomechanics, and adsorption phenomenon was proposed to characterize gas flow in the shale reservoir. Firstly, the characteristics of shale gas reservoirs are analyzed, and the physical parameters of gas at high pressure and high temperature are calculated by using the Peng–Robinson state equation. Secondly, the seepage mathematical model is solved

by using finite difference, and the results are compared with commercial software. Furthermore, the correction coefficient of shale permeability with stress sensitivity and multiscale seepage is discussed under different pressures and pore sizes. Finally, to evaluate the impact of stress sensitivity, adsorption, and porosity on the shale gas mechanism, several cases concerning production dynamics of multistage fractured horizontal wells have been carried out.

## 2. Shale Reservoir Characterization

With the application of high-resolution electron microscopy in investigation of shale pore structures, some studies have illustrated that the pore structure of shale is complex and behaviors show strong heterogeneity, and the pore types in shale are classified as intergranular pores, intragranular pores, some dissolved pores, and microfractures [7, 8]. Due to the difference and diversity of pore development, the distribution of the shale pore diameter varies from 1 nm to 1000 nm [9–11]. Moreover, the results of core analysis show that the permeability of shale varies from $10^{-6}$ mD to 1 mD [11]. In a word, the physical property and structural characteristics of the shale reservoir directly affect the transportation mechanism of shale gas. The physical model of shale gas production and transport is shown in Figure 1. Matrix pores, natural microfractures, and hydraulic fractures consist of the network channel for gas transfer [11]. Among them, the matrix accounts for the main reservoir space, and the fracture plays a key role in the transportation channel. Free gas and adsorbed gas transport from natural fractures to hydraulic fractures under pressure difference. In addition, when gas migrates in the nanoscale pore, the gas molecules collide seriously with the pore roaring wall of the shale, slippage, transition, and free-molecular flow will be included in microscale and nanosacle pore space besides Darcy flow. Therefore, the transportation of shale gas involves different spatial scales.

The occurrence state of shale gas can be divided into the form of adsorption gas, free gas, and dissolution gas. And several investigations have illustrated that the adsorption gas may account for 20%~80% of the total reserves in shale gas [12]. Thus, the adsorption capacity of shale is very important for shale gas reservoir evaluation, and the physical changes of adsorption gas may have an important impact on shale production behaviors. To characterize the relationship between adsorbed gas and pressure in shale reservoirs, a mass of experiments have been done to understand the characteristics of shale gas absorption in recent years. And several models are proposed to characterize the shale gas adsorption phenomenon. Specially, the Langmuir adsorption equation has been widely used because of its simple form and slight error [12, 13]. Furthermore, the parameters of the Langmuir equation can be easily obtained by fitting the experimental data. The mathematical form of rock adsorption volume $V_E$ is represented as follows:

$$V_E = V_L \frac{P}{P + P_L}, \tag{1}$$

where $V_L$ and $P_L$ is the Langmuir pressure and Langmuir volume, respectively, which can be obtained by fitting the isothermal adsorption experimental data, and the isothermal adsorption curve of shale measured in the laboratory is shown in Figure 2.

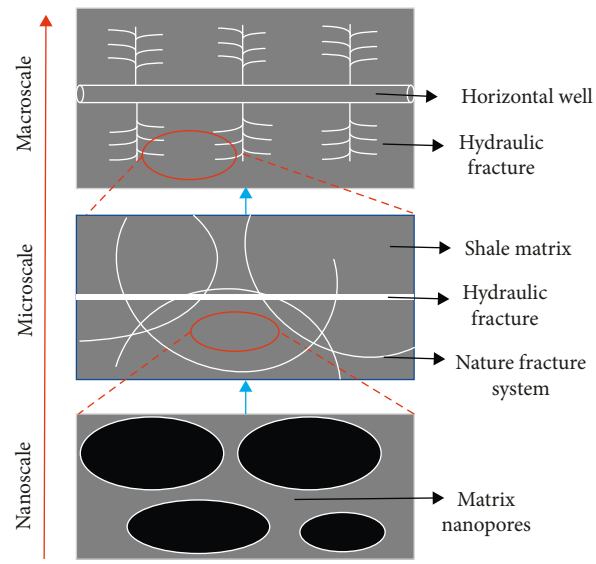


Figure 1: Physical model of gas transport.

In fact, there is no difference in the composition between the adsorbed gas and the free gas. According to the component analysis of the shale gas produced, the study shows that the shale gas is a natural gas mainly composed of methane, and the methane content is up to 98% [14]. It is a typical dry gas reservoir. With the change of temperature and pressure, the methane state is divided into the solid state, liquid state, gaseous state, and supercritical state [15]. As shown in Figure 3, it can be seen from that the actual shale reservoir temperature is much higher than the critical temperature of methane, which means the shale gas is in a supercritical state.

In addition, we calculate the high-pressure physical parameters of methane by the Peng–Robinson equation of state [16], which is expressed as follows:

$$p = \frac{RT}{v - b} - \frac{a(T)}{v(v + b) + b(v - b)}, \tag{2}$$

where

$$\begin{aligned} a(T) &= \alpha(T) \cdot a_c, \\ a_c &= \frac{0.45724 R^2 T_c^2}{p_c}, \\ b &= \frac{0.07780 R T_c}{p_c}, \\ \alpha(T) &= \left[1 + m\left(1 - T_r^{0.5}\right)\right]^2, \\ m &= 0.37464 + 1.54226\omega - 0.2699\omega^2. \end{aligned} \tag{3}$$

Besides, the equation can also be written as follows:

$$Z^3 - (1 - B)Z^2 + \left(A - 2B - 3B^2\right)Z - \left(AB - B^2 - B^3\right) = 0, \tag{4}$$

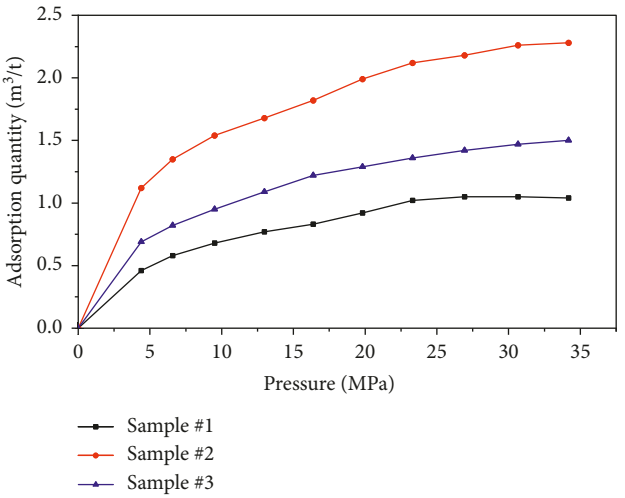


Figure 2: Isothermal adsorption curve of shale.

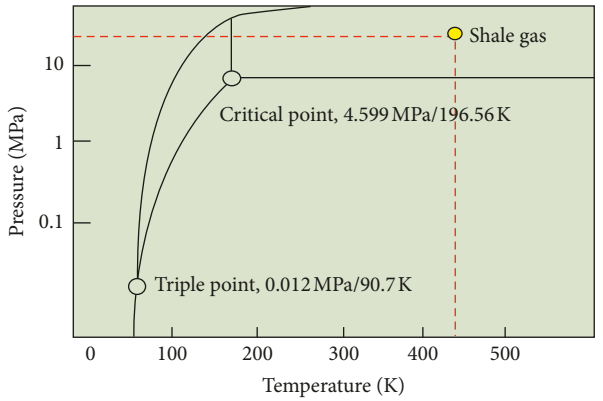


Figure 3: Phase diagram of methane.

where

$$A = \frac{ap}{R^2T^2},$$
$$B = \frac{bp}{RT}. \tag{5}$$

The gas density can be calculated:

$$\rho_g = \frac{M}{v} = \frac{pM}{ZRT}. \tag{6}$$

And gas viscosity is calculated by Lee's empirical model [17]:

$$\mu_g = 10^{-7}K\exp\left(X\left(10^{-9}\rho_g\right)^Y\right), \tag{7}$$

where

$$K = \frac{\left(9.379 + 0.016M_g\right)(1.8T)^{1.5}}{209 + 19M_g + 1.8T},$$
$$X = 3.448 + \frac{986.4}{1.8T} + 0.01M_g, \tag{8}$$
$$Y = 2.447 - 0.2224X.$$

The calculation results are shown in Figures 4–6, including deviation factor, density, and viscosity. This part of work provides gas physical parameters for establishing the transport model of the shale gas reservoir.

## 3. Mathematical Model

*3.1. Apparent Permeability Model with Stress Sensitivity.* To describe the variation of gas transport in porous media, researchers have proposed to use the Knudsen number to classify the shale gas flow regime [18]. Knudsen number was defined as the ratio of mean free path of gas molecules to pore size of porous media. Flow regimes are divided into four categories, as shown in Table 1. Figure 7 is the Knudsen number corresponding to different pore sizes under different pressure conditions. It can be seen that the flow regime includes continuous flow, slippage flow, and transition flow in the shale gas reservoir. Therefore, the transport mechanism in shale could not be characterized by the classical Darcy law.

So, an apparent permeability model based on Beskok–Karniadakis (BK model) theory is widely used to characterize the multiscale transport of shale gas [19–24], and the model can be expressed as follows:

$$k_{app} = \left(1 + \frac{128}{15\pi^2}\tan^{-1}\left(4K_n^{0.4}\right)K_n\right)\left(1 + \frac{4K_n}{1 - bK_n}\right)k_0. \tag{9}$$

Furthermore, when the pressure changes during the transportation of shale gas in porous media, the stress sensitivity and adsorption will cause the variation of shale pore radius, which lead to the change of shale apparent permeability. In view of the above phenomenon, Guo et al. [25] modified the Beskok–Karniadakis permeability model (BKG model) based on the capillary bundle model. And the modified Beskok–Karniadakis permeability model can be illustrated as follows:

$$k_{as} = \frac{r_e^4}{r_0^4}\left[1 + \frac{128}{15\pi^2}\tan^{-1}\left(4K_{ne}^{0.4}\right)K_{ne}\right]\left(1 + \frac{4K_{ne}}{1 - bK_{ne}}\right)k_0, \tag{10}$$

where

$$K_{ne} = \frac{\lambda}{r_e},$$
$$r_e = r_0 + \Delta r_{desorption} + \Delta r_{stress},$$
$$\Delta r_{desorption} = \chi\frac{p_i}{p_i + p_L} - \chi\frac{p}{p_i + p_L}, \tag{11}$$
$$\Delta r_{stress} = \left(e^{-(a/4)\sigma_{eff}} - 1\right)r_0,$$

where $\sigma_{eff}$ is the effective stress rock, which can be calculated as follows:

$$\sigma_{eff} = \sigma - p. \tag{12}$$

To clearly understand the effect of stress sensitivity and adsorption on apparent permeability, the correction coefficient of permeability $\xi$ is defined in the following form:

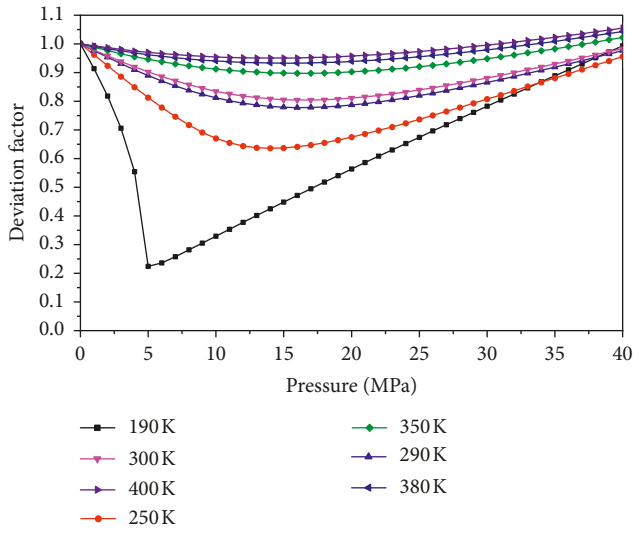


Figure 4: Deviation factor of methane.

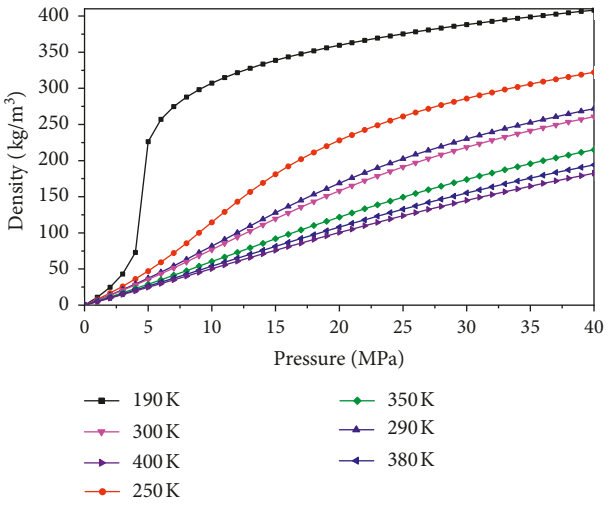


Figure 5: Mass density of methane.

$$\xi = \frac{k_{as}}{k_0} = \frac{r_e^4}{r_0^4}\left[1 + \frac{128}{15\pi^2}\tan^{-1}\left(4K_{ne}^{0.4}\right)K_{ne}\right]\left(1 + \frac{4K_{ne}}{1 - bK_{ne}}\right). \quad (13)$$

*3.2. Multiscale Transport Model of Shale Gas.* In consideration of the actual reservoir formation containing nature fracture networks and matrix porosity, the matrix and the fracture system are equivalent to a porous medium. Additionally, to make this mathematical model more tractable and easier to understand, the following assumptions are made:

(1) The gas component is only methane, and it flows at a constant temperature.

(2) The gas exists in the form of adsorption and free. And the desorption phenomenon can be characterized by Langmuir isothermal adsorption theory; moreover, the process of desorption and adsorption can reach an instant balance.

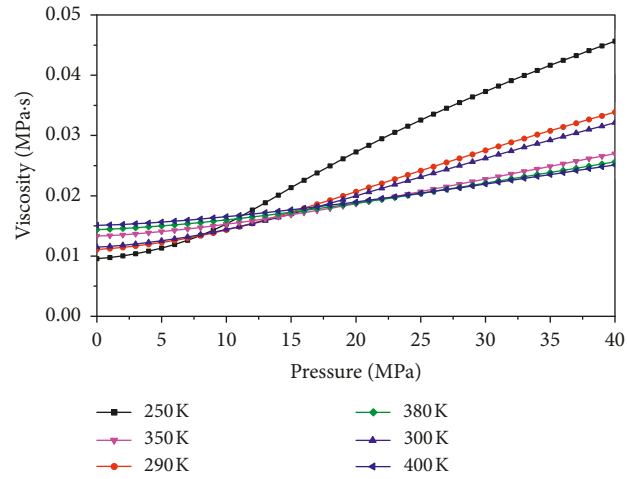


Figure 6: Viscosity of methane.

Table 1: Division of flow regimes according to the Knudsen number.

| Knudsen number | Flow regime |
|---|---|
| 0~0.001 | Continue flow |
| 0.001~0.1 | Slip flow |
| 0.1~10 | Transition flow |
| >10 | Free-molecular flow |

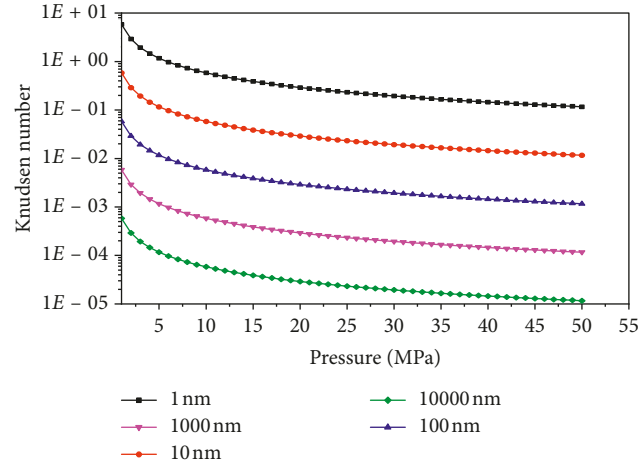


Figure 7: Knudsen number of different pore sizes and pressures ($T = 400$ K).

(3) Gas reservoir model is homogeneous and isotropic, ignoring the compressibility of rock.

(4) The effect of reservoir stress sensitivity and desorption on shale permeability is taken into account.

Based on the above assumptions and according to the law of mass conservation, the continuity equation of shale gas can be derived as follows:

$$-\nabla \cdot \left(\rho_g \vec{v}\right) - q_g = \frac{\partial\left(\phi\rho_g\right)}{\partial t} + \frac{\partial\left[\rho_{gsc}\rho_f V_L p/\left(p + p_L\right)\right]}{\partial t}. \quad (14)$$

The generalized Darcy law based on apparent permeability is expressed as follows:

$$\overrightarrow{v} = -\frac{k_{as}}{\mu_g}\left(\nabla p - \rho_g g \nabla Z\right). \tag{15}$$

Substituting equation (15) into equation (14), we can obtain the governing equation of multiscale migration of shale gas considering stress sensitivity:

$$\nabla \cdot \left[\frac{k_{as}\rho_g}{\mu_g}\left(\nabla p - \rho_g g \nabla Z\right)\right] - q_g = \frac{\partial\left(\phi\rho_g\right)}{\partial t} + \frac{\partial\left[\rho_{gsc}\rho_f V_L p/\left(p + p_L\right)\right]}{\partial t}. \tag{16}$$

Initial conditions and boundary conditions should be added to solve the partial differential equation. The initial condition of the gas reservoir is the distribution of pressure at each point. Since the gas is in a static equilibrium state before transport, the pressure at any position is the original formation pressure:

$$p(x, y, z)|_{t=0} = p_i. \tag{17}$$

When there is no edge and bottom water around reservoir, it can be considered that the gas reservoir is a closed boundary condition, which is mathematically known as the second boundary condition or Neumann boundary condition:

$$\left.\frac{\partial p}{\partial n}\right|_{\Gamma} = 0. \tag{18}$$

According to the working system of the actual shale gas production wells, the inner boundary conditions usually include the conditions of fixed-output gas quantity and fixed-bottom flow pressure production. As we all know, the well radius is far less than the well distance, and thus, the production well is treated as the source in the numerical simulation. When the bottom hole pressure is determined, the Peaceman well model can be adopted to correspond the bottom hole flow pressure and gas production volume, and then, the source term or sink term can be added to the differential equation [26], which can be describes as follows:

$$Q_g = \frac{2\pi k_{as} h}{u_g\left(\ln\left(r_e/r_w\right) + S\right)}\left(p_{i,j,k} - p_{wf}\right). \tag{19}$$

As for isotropic formations, the equivalent supply radius is

$$r_e = 0.14\sqrt{\Delta x^2 + \Delta y^2}. \tag{20}$$

*3.3. Numerical Solutions of Mathematical Model.* In this part, the finite difference method is used to discretize the above differential equation of shale gas seepage flow. And local grid refinement is used to describe the hydraulic fractures. Figure 8 represents a simplified numerical simulation flowchart of shale gas seepage in the porous media. To approve the accuracy of the developed numerical model presented in this paper, production behavior for a vertical well in a convention gas reservoir is calculated with a simple case of the presented model, and the results are validated with commercial software, which is an adaptive implicit black oil simulator. The basic parameters for the gas reservoir model are shown in Table 2. Gas adsorption, multiscale flow mechanism, and stress sensitivity are not considered in the model. Figure 9 represents the match result of gas production rate, and Figure 10 shows the distribution of pressure on model profile. Simulation results of this work match well with the commercial simulation software.

## 4. Results and Discussion

*4.1. Apparent Permeability Analysis in Shale Gas.* In this section, the effect of stress sensitivity and adsorption on apparent permeability in the shale matrix is discussed. The basic parameters for the seepage model are shown in Table 3.

The relationship between permeability correction coefficient and pressure under a different pore size without stress sensitivities is shown in Figure 11(a). It is can be clearly found that the correction coefficient of permeability is greater than 1 without considering the stress sensitivity and adsorption, which means the apparent permeability of shale is greater than the intrinsic permeability. Additionally, the correction coefficient of permeability decreases with the increase of pore size, and the reason is that the effect of stress and the increase of pore size reduce the Knudsen number; thus, the gas flow in porous media is in continuous flow, and apparent permeability and absolute permeability reach a consensus.

Besides, the relationship between permeability correction coefficient and pressure under a different pore size with stress sensitivity equal to $0.06\,\mathrm{MPa}^{-1}$ is shown in Figure 11(b). It reveals that the apparent permeability is affected by the stress sensitivity; specifically, when the pore diameter is greater than 5 nm, the permeability correction coefficient decreases first and then rises with the decrease of pressure. When the pore diameter is less than 5 nm, the permeability correction coefficient increases with the decrease of pressure. These results are in accordance with findings of earlier investigations [25]. In a word, compared with the BK model, BKG model can characterize the multiscale seepage mechanism in shale gas when considering the effective stress variation [27, 28].

*4.2. Effect of Stress sensitivity.* In this section, the influence of stress sensitivity for gas transport in shale matrix and fracture is investigated thoroughly, and the basic parameters for the multistage fractured horizontal well numerical simulation are listed in Table 4. The parameters in Table 4 are derived from a horizontal well in Fuling Shale Gas Field, China. In order to increase the calculation efficiency, only three hydraulic fractures are considered. And the 3D shale gas reserve model with a multistage horizontal well is represented in Figure 12. In the basic case, the shale stress

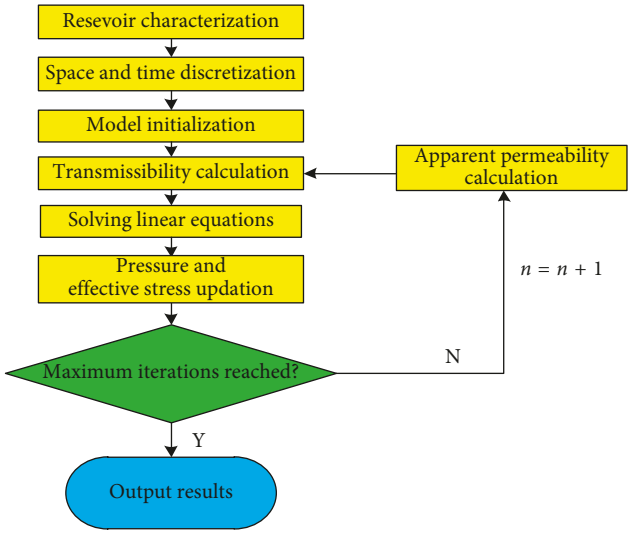


Figure 8: Numerical simulation process.

Table 2: Gas reservoir parameters for validation.

| Parameter | Value |
|---|---|
| Initial reservoir pressure, $p_i$ | 300 MPa |
| Formation temperature, $T$ | 363 K |
| Porosity, $\phi$ | 0.12 |
| Permeability, $K$ | 0.5 mD |
| Reservoir area, $A$ | $210 \times 210\ m^2$ |
| Thickness, $h$ | 30 m |
| Grid dimension, $N_x \times N_y \times N_z$ | $21 \times 21 \times 1$ |
| Wellbore pressure, $p_{wf}$ | 8 MPa |
| Wellbore radius, $r_w$ | 0.1 m |

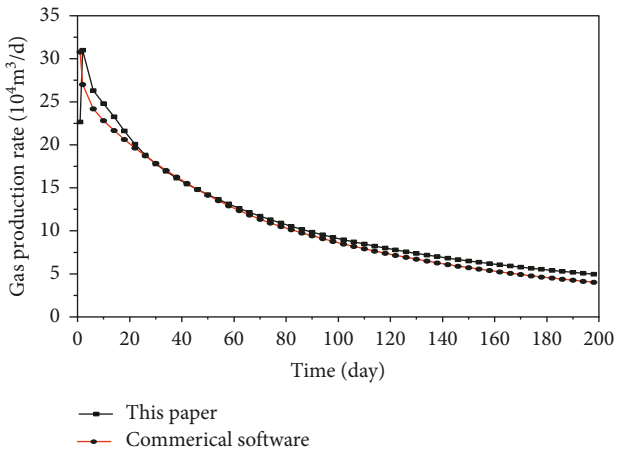


Figure 9: The match result of the gas productive rate.

sensitivity coefficient is 0, which means there is no stress sensitivity. In addition, we keep the parameters of the reservoir and multistage as a constant while change the stress sensitivity coefficient. Through these scenarios, we can obtain the impacts of the stress sensitivity on the multistage horizontal well interstitial flow.

The simulation results of the behavior of multistage fractured horizontal well in a 500 days period for the four

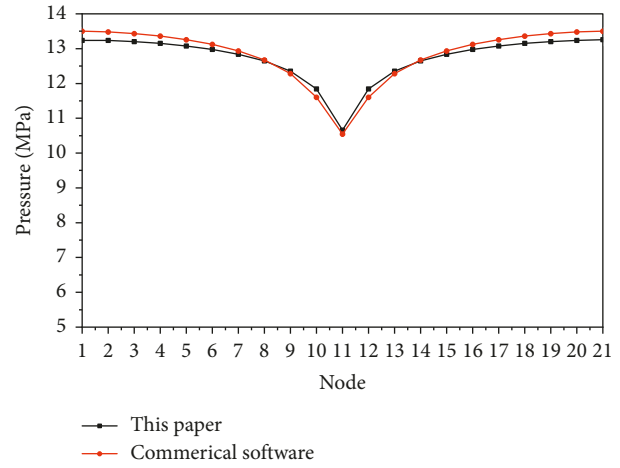


Figure 10: The distribution of pressure on the gas reservoir profile after 200 days.

Table 3: Basic parameters for the seepage model.

| Parameter | Value |
|---|---|
| Initial reservoir pressure, $p_i$ | 50 MPa |
| Formation temperature, $T$ | 363 K |
| Thickness of the adsorption layer, $\chi$ | $0.38 \times 10^{-9}$ m |
| Slip coefficient, $b$ | −1 |
| Langmuir pressure, $P_L$ | 5 MPa |
| Stress sensitivity coefficient, $a$ | 0.06 MPa$^{-1}$ |

cases are shown in Figures 13(a) and 13(b). It is noticeable that the gas production rate and cumulative gas production will decrease when the shale gas reservoir stress sensitivity coefficient increases. The reason is that increasing stress sensitivity coefficient means there are more deformation for the shale rock skeleton, and it can reduce shale gas apparent permeability. The simulation case without stress sensitivity has the biggest cumulative gas production of about $3011 \times 10^4$ m$^3$ after 500 days, while for the case of stress sensitivity coefficient 0.12 MPa$^{-1}$, the cumulative gas production is about 0.41 times of that value. In conclusion, the stress sensitivity has an important effect on shale gas transport, and the deformation of the rock skeleton will affect the behaviors of multistage horizontal well in shale gas.

Specially, we analyzed the multiscale seepage mechanism in shale gas with the case of stress sensitivity, namely, 0.03 MPa$^{-1}$, 0.05 MPa$^{-1}$, and 0.12 MPa$^{-1}$. Figure 14 represents the pressure distribution at different times with stress sensitivity coefficient equal to 0.05 MPa$^{-1}$. It is clearly seen that the shale matrix pressure evolution of the case of coefficient is 0.05 MPa$^{-1}$. The process of shale gas transportation can be divided into three stages. Firstly, the gas in the fractured shale area flows into the wellbore. Secondly, the matrix gas flows into the hydraulic fracture. Then, the gas within the kerogen will undergo desorption and diffusion to the matrix pore. Figures 15(a) and 15(b) show the distribution of the permeability correction factor under different stress sensitivity coefficients after 500 days. These results demonstrate that stress sensitivity coefficient can reflect the impact degree from effective stress, and the shale gas matrix

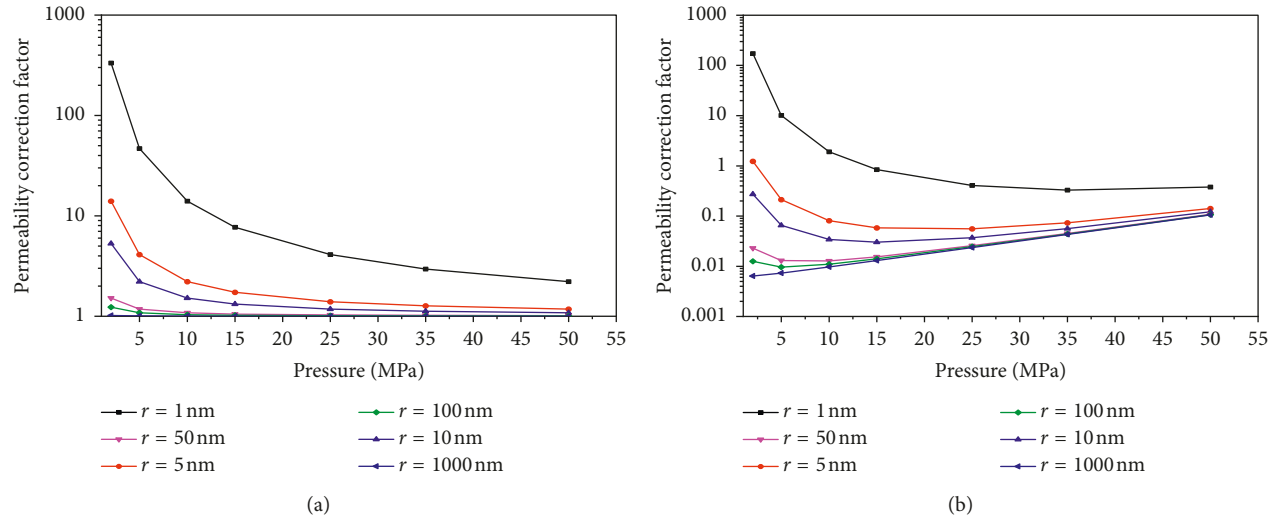


Figure 11: The relationship between permeability correction coefficient and pressure: (a) without stress sensitivity; (b) with stress sensitivity.

Table 4: Main parameters for gas reservoir simulation.

| Parameters | Value |
|---|---|
| Initial reservoir pressure, $p_i$ | 35 MPa |
| Formation temperature, $T$ | 363 K |
| Porosity, $\phi$ | 0.05 |
| Permeability, $K$ | 0.005 mD |
| Reservoir dimension, $A$ | $700 \times 1860$ m$^2$ |
| Thickness, $h$ | 35 m |
| Dimension, $N_x \times N_y \times N_z$ | $25 \times 126 \times 1$ |
| Rock density, $\rho_f$ | 2500 kg/m$^3$ |
| Langmuir pressure, $P_L$ | 5 MPa |
| Langmuir volume, $V_L$ | $4 \times 10^{-3}$ m$^3$/kg |
| Adsorption layer thickness, $\chi$ | $0.38 \times 10^{-9}$ m |
| Wellbore radius, $r_w$ | 0.1 m |
| Bottom hole pressure, $p_{wf}$ | 10 MPa |
| Horizontal well length, $L$ | 800 m |
| Hydraulic fracture half-length, $L_f$ | 130 m |
| Number of fractures, $n_f$ | 3 |
| Conductivity, $K_f w_f$ | 1 mD·m |

permeability will decrease after gas production, which leads to increase the seepage resistance and decrease the gas flowing into wellbore. So, in order to avoid the effect of stress sensitivity on shale gas production, reasonable production pressure difference should be investigated considered particularly.

*4.3. Effect of Adsorption Phenomenon.* In this study, we perform sensitivity analysis of the absorption volume. Four cases are proposed to investigate the impact of the absorption on shale gas multiscale transport. The Langmuir pressure is treated as a constant, while the Langmuir volume is changed. To be specific, four cases of Langmuir volume, namely, 0 m$^3$/kg, 0.004 m$^3$/kg, 0.008 m$^3$/kg, and 0.012 m$^3$/kg, are analyzed. Other reservoir parameters are same, and the simulation results are shown in Figures 16(a) and 16(b); it can clearly be found that gas production rate and cumulative gas production increase with an increase in Langmuir volume. And the cumulative gas produced increases by 1.6% and 4.3% for the Langmuir pressure from 0.004 to 0.008 and 0.012, respectively. The reason is that an increase in the Langmuir volume means an increase in adsorbed gas reserves; moreover, when the pressure drops, the adsorbed gas is desorbed to free gas, which supplements the formation energy. In summary, the adsorption phenomenon has an influence on shale gas seepage and sorption capacity, which is an important effect to analyze the multistage fractured horizontal well production behavior; however, the effect of adsorption is very weak in the early gas transport period, and the impact will increase later.

*4.4. Impact of Shale Porosity.* Three separate simulation cases were validated with shale porosity of 0.01, 0.05, and 0.10. The results of multistage fractured horizontal well behavior are presented in Figures 17(a) and 17(b). It can clearly be found that the significance difference in gas production rate decline is apparent between the models. Furthermore, the cumulative gas production has been increased to 1.6 times with the porosity increased from 0.05 to 0.1. And the difference of shale matrix porosity can affect the Knudsen number of grids, as shown in Figures 18(a) and 18(b). Knudsen gradually increases with the decrease of pressure. With the continuous decrease of pressure, the flow pattern of gas transits from continuous flow to slippage and transition flow. Because the Knudsen number is the function of pressure, large pressure drop on the fracture leads to large number of Knudsen around the fracture. These results highlight the importance of matrix porosity to shale gas productivity. The reason is that the larger the storage space the shale matrix has, the more the free gas it contains, which can delay the decline of formation energy.

*4.5. Impact of Fracture Length and Conductivity.* In this section, we perform sensitivity analysis of the fracture length

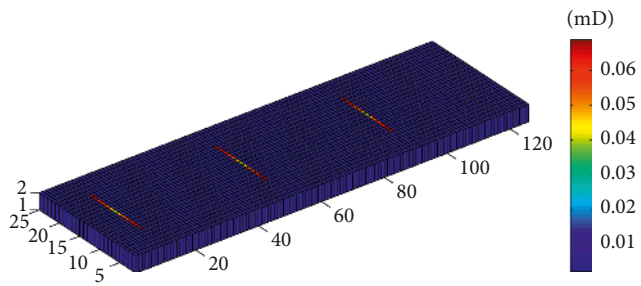


Figure 12: Shale gas reservoir simulation model (permeability distribution).

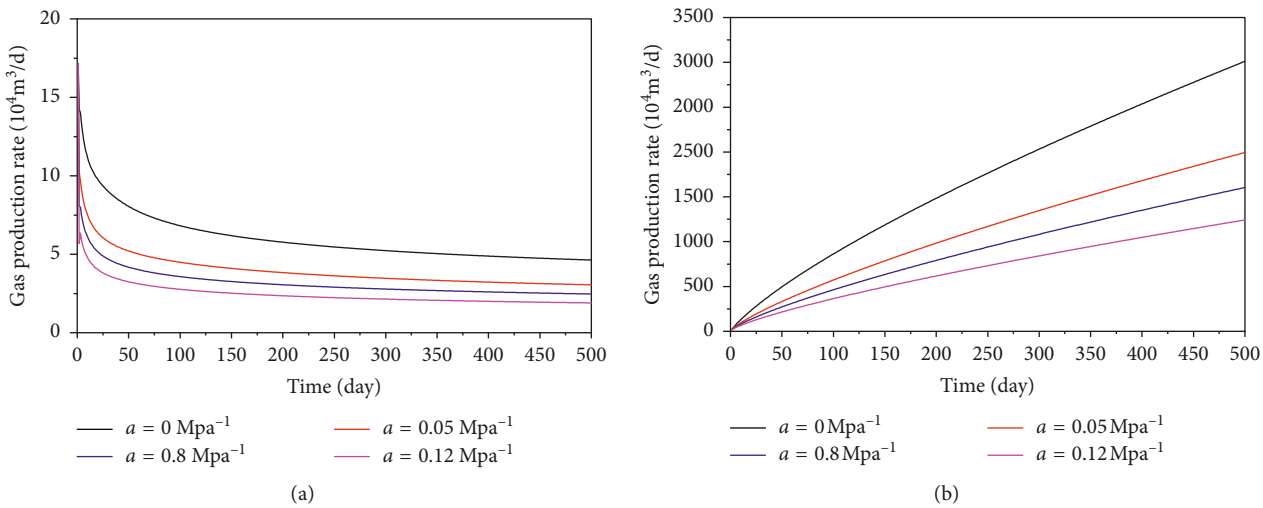


Figure 13: The behavior of the multistage fractured horizontal well: (a) gas production rate; (b) cumulative gas production.

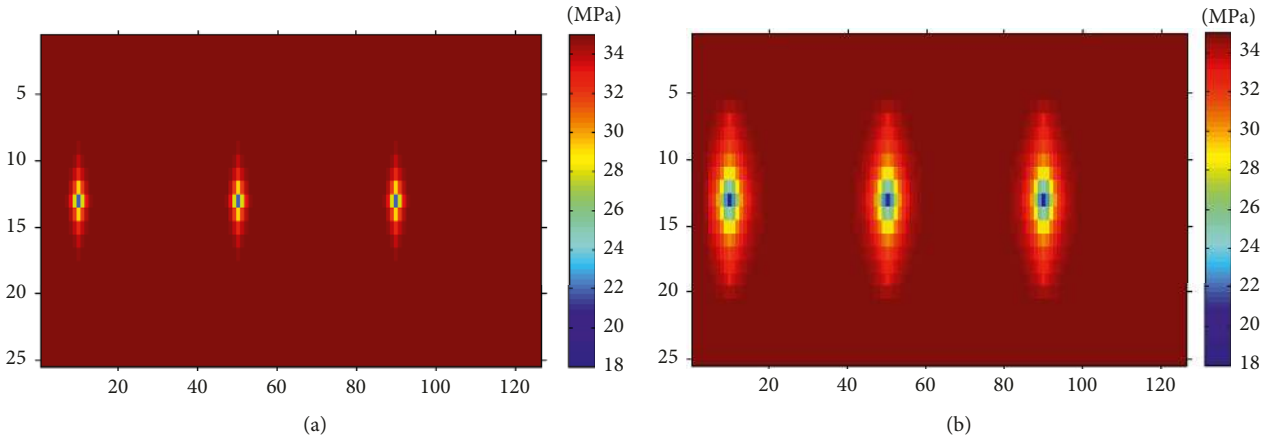


Figure 14: Continued.

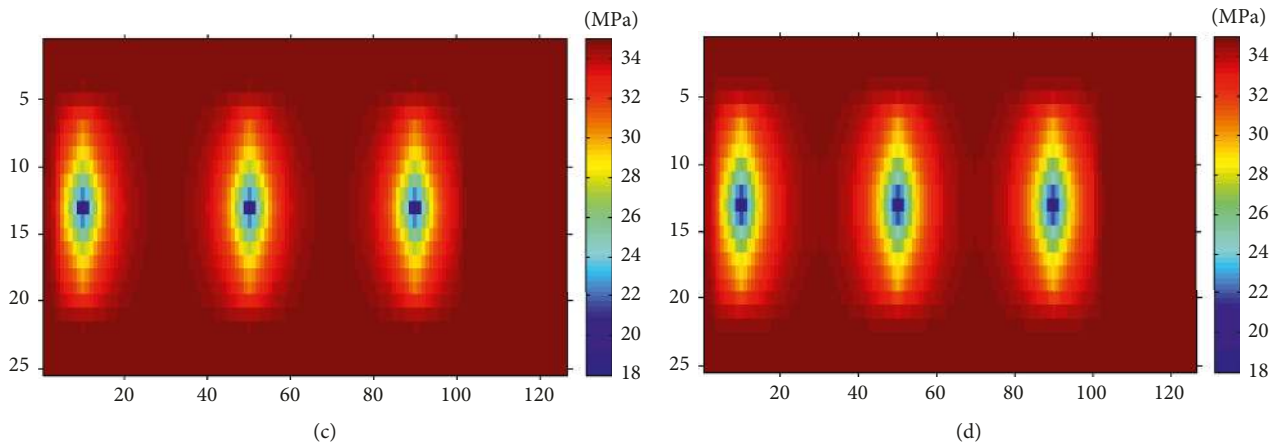


Figure 14: Distribution of shale matrix pressure: (a) $t = 10$ days; (b) $t = 100$ days; (c) $t = 350$ days; (d) $t = 500$ days.

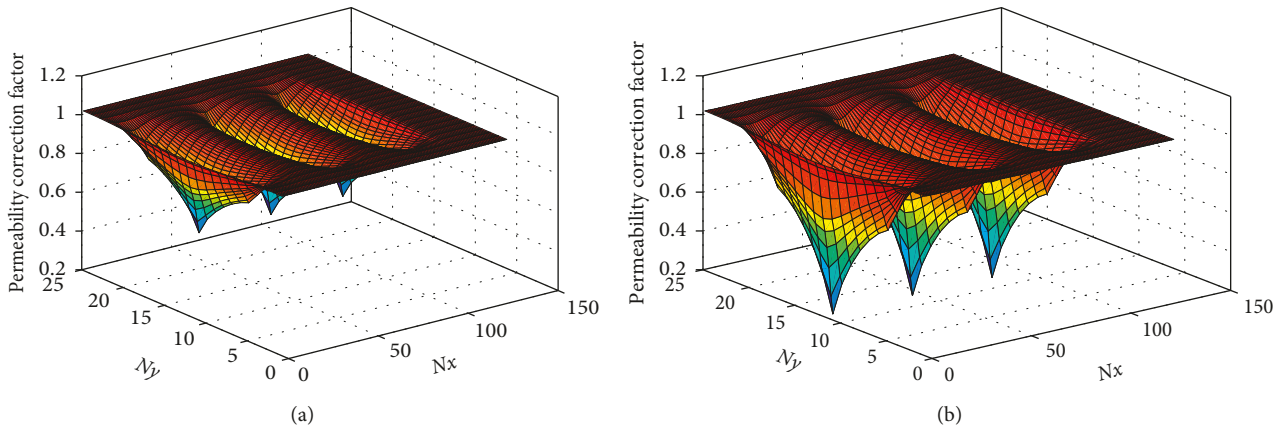


Figure 15: Distribution of the permeability correction factor after 500 days: stress sensitivity coefficient equals (a) 0.03 $MPa^{-1}$ and (b) 0.12 $MPa^{-1}$.

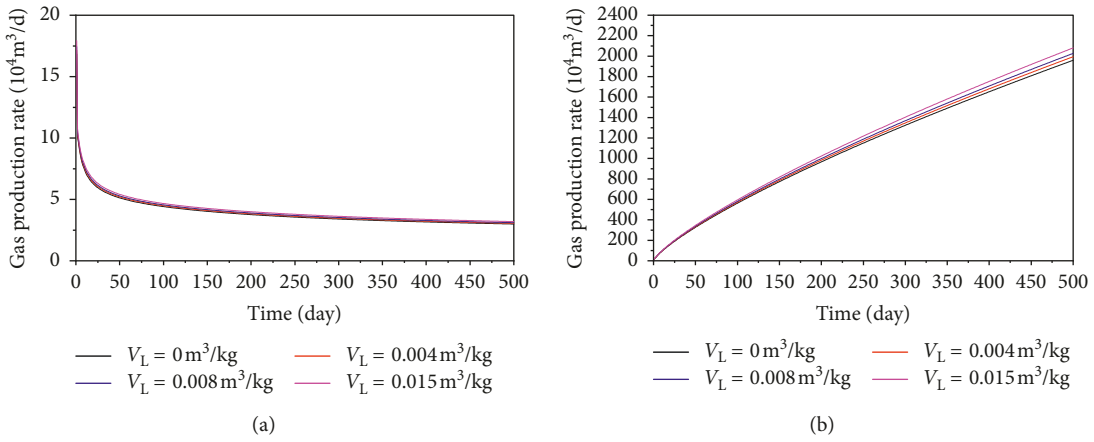


Figure 16: Effect of Langmuir volume on behavior of the multistage fractured horizontal well: (a) gas production rate; (b) cumulative gas production.

and conductivity. The effect of fracture length on gas production rate and cumulative gas production is shown in Figures 19(a) and 19(b). The effect of fracture conductivity on gas production rate and cumulative gas production is shown in Figures 20(a) and 20(b). Cumulative shale gas production increases with the length of fracture. It can be clearly found that cumulative gas production increases with the increase of fracture length and conductivity.

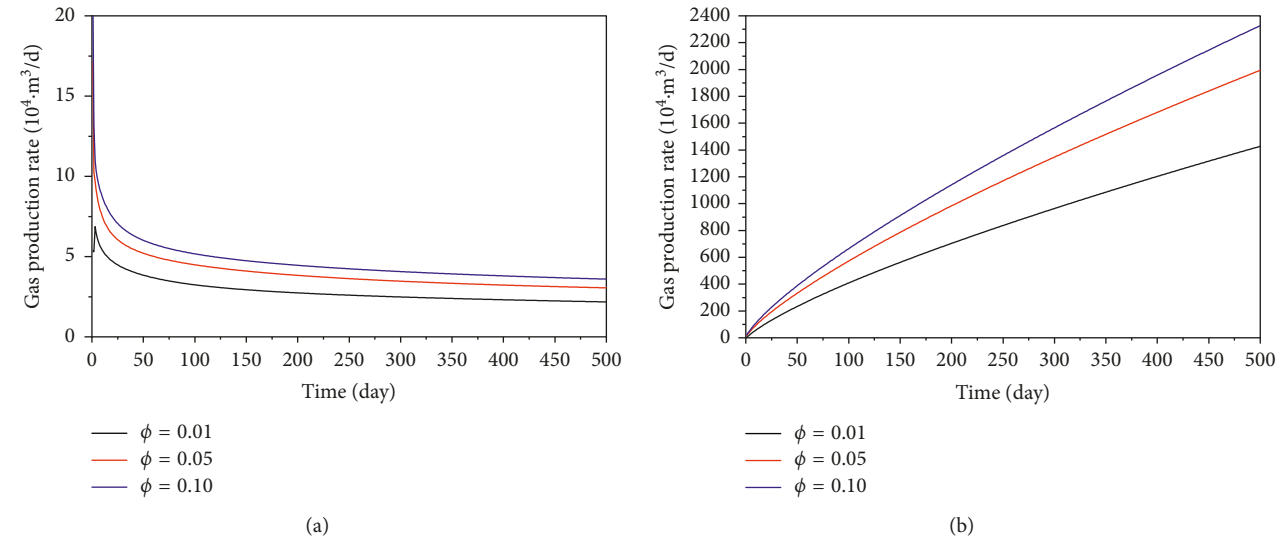


Figure 17: Effect of porosity on behavior of the multistage fractured horizontal well: (a) gas production rate; (b) cumulative gas production.

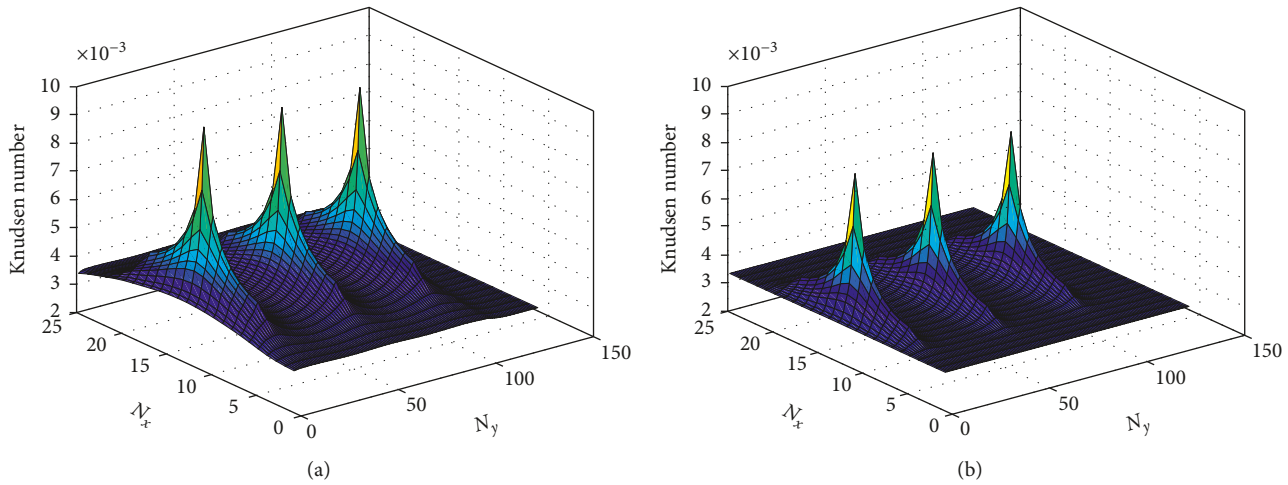


Figure 18: Distribution of Knudsen after 500 days with shale porosity equal to (a) 0.01 and (b) 0.10.

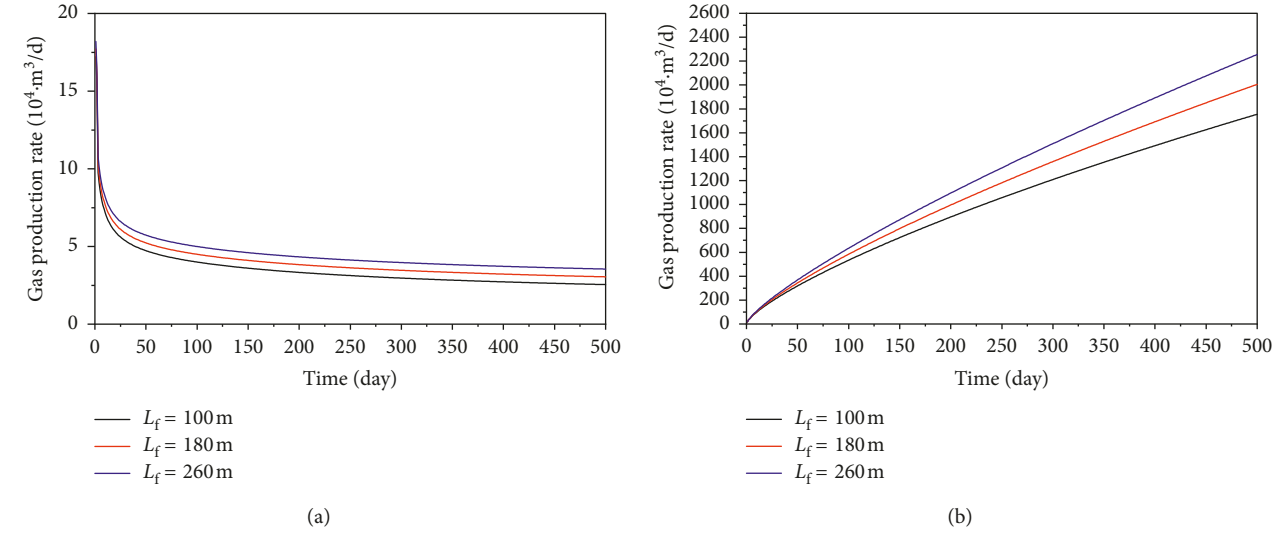


Figure 19: Effect of fracture length on behavior of the multistage fractured horizontal well: (a) gas production rate; (b) cumulative gas production.

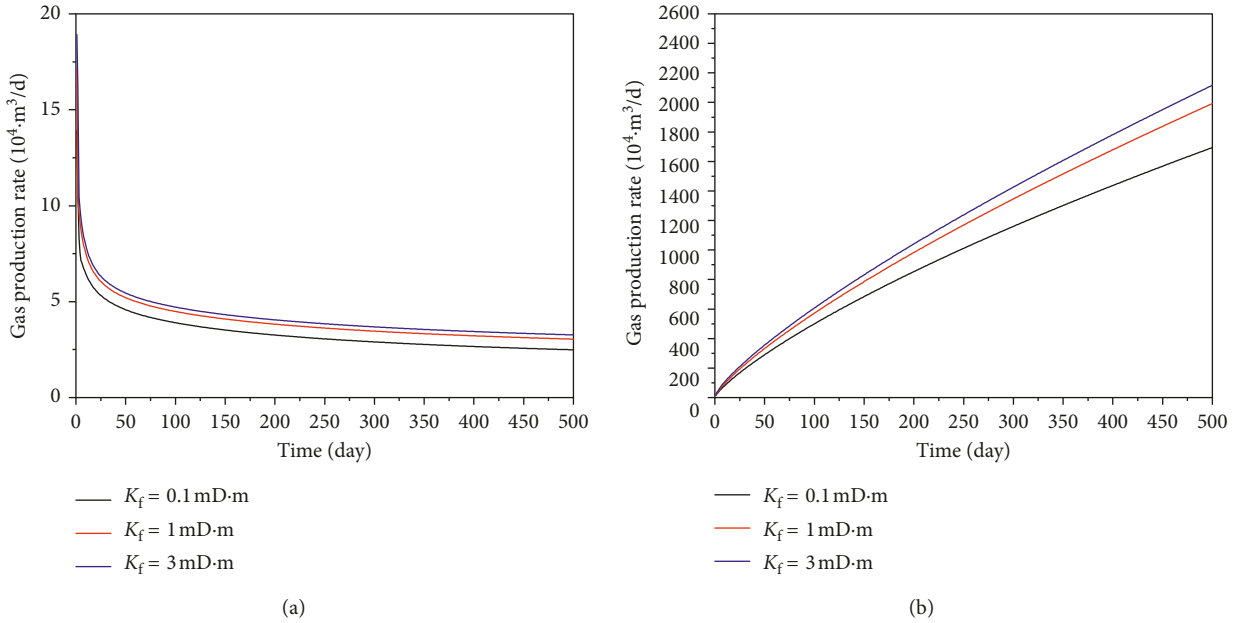


Figure 20: Effect of fracture conductivity on behavior of the multistage fractured horizontal well: (a) gas production rate; (b) cumulative gas production.

## 5. Conclusions

In this paper, a model of gas multiscale transportation-coupled stress sensitivity is proposed to investigate the shale gas seepage mechanism. The mathematical model is solved using the finite difference method. According to the analysis of key parameters, the following conclusions can be deduced:

(1) A new apparent permeability model considering multiscale flow and stress sensitivity was proposed and analyzed. Pore size and stress sensitivity have an important influence on the permeability correction factor. The stress sensitivity can lead to the decrease of shale permeability.

(2) The behavior of the multistage fractured horizontal well is simulated with a different stress sensitivity coefficient. The stress sensitivity actually has a significant impact on shale gas multiscale seepage. The gas production rate and cumulative gas production will decrease when the shale gas reservoir stress sensitivity coefficient increases, and the stronger the stress sensitivity, the lower the recovery factor of shale gas.

(3) The Langmuir pressure and shale porosity significantly affect the behavior of the multistage fractured horizontal well. The cumulative shale gas increases as the Langmuir volume and porosity increase. However, the variation of porosity has more obvious effect on gas production than Langmuir volume in the early period.

(4) The Langmuir pressure and shale porosity significantly affect the behavior of the multistage fractured horizontal well. The cumulative shale gas increases as the Langmuir volume and porosity increase. And cumulative gas production increases with the increase of fracture length and conductivity. And the variation of porosity has more obvious effect on gas production than Langmuir volume in the early period.

## Nomenclature

| | |
|---|---|
| $k_{app}$: | Shale apparent permeability (mD) |
| $k_0$: | Shale intrinsic permeability (mD) |
| $\phi$: | Shale reservoir porosity |
| $K_{ne}$: | Effective Knudsen number, $K_{ne} = \lambda/r_e$ |
| $b$: | Slip coefficient |
| $r_e$: | Pore average effective radius (m) |
| $\Delta r_{desorption}$: | Variation of pore radius due to desorption (m) |
| $\Delta r_{stress}$: | Variation of pore radius due to stress sensitivity (m) |
| $p_L$: | Langmuir pressure (MPa) |
| $p$: | Reservoir pressure (MPa) |
| $p_i$: | Initial reservoir pressure (MPa) |
| $V_L$: | Langmuir volume (m$^3$/kg) |
| $\chi$: | Thickness of the adsorption layer (m) |
| $a$: | Stress sensitivity coefficient (1/MPa) |
| $\sigma_{eff}$: | Effective stress (MPa) |
| $\sigma$: | External stress (MPa) |
| $\rho_f$: | Density of rock skeletons (kg/m$^3$) |
| $\rho_g$: | Gas density in formation (kg/m$^3$) |
| $\rho_{gsc}$: | Gas density (kg/m$^3$) |
| $\mu_g$: | Gas viscosity in formation (mPa·s) |
| $Q_g$: | Gas production rate (m$^3$/d) |
| $\Delta x$: | Grid step in the $x$ direction (m) |
| $\Delta y$: | Grid step in the $y$ direction (m) |
| $r_e$: | Equivalent supply radius (m). |

## Data Availability

The simulation data used to support the findings of this study are available from the corresponding author upon request.

## Conflicts of Interest

The authors declare that they have no conflicts of interest.

## Acknowledgments

This work was financially supported by Major National Science and Technology Projects (Grant no. 2016ZX05060-009) and China Petroleum Science Technology Innovation Fund (Grant no. 2016D-5007-0208). Besides, the authors would like to acknowledge Dr. Jing Sun and Professor Dehua Liu for their immense polishing skills and contribution to this paper.

## References

[1] T. Huang, X. Guo, and K. Wang, "Nonlinear seepage model of gas transport in multiscale shale gas reservoirs and productivity analysis of fractured well," *Journal of Chemistry*, vol. 2015, Article ID 349507, 10 pages, 2015.

[2] I. Shovkun and D. N. Espinoza, "Coupled fluid flow-geomechanics simulation in stress-sensitive coal and shale reservoirs: impact of desorption-induced stresses, shear failure, and fines migration," *Fuel*, vol. 195, pp. 260–272, 2017.

[3] L. Zhang, B. Shan, Y. Zhao, J. Du, J. Chen, and X. Tao, "Gas transport model in organic shale nanopores considering Langmuir slip conditions and diffusion: pore confinement, real gas, and geomechanical effects," *Energies*, vol. 11, no. 1, p. 223, 2018.

[4] K. Wu, Z. Chen, and X. Li, "Real gas transport through nanopores of varying cross-section type and shape in shale gas reservoirs," *Chemical Engineering Journal*, vol. 281, pp. 813–825, 2015.

[5] R. Zhang, Z. Ning, F. Yang, and H. Zhao, "Shale stress sensitivity experiment and mechanism," *Acta Petrolei Sinica*, vol. 36, pp. 224–231, 2015.

[6] H. Yin, E. Zhao, L. Wang, H. Zhao, and J. Fu, "Pressure behavior analysis for vertical fractured well with stress sensitivity in shale gas reservoirs," *Chinese Journal of Hydrodynamics*, vol. 30, pp. 412–417, 2015.

[7] J. Yan, S. Zhang, J. Wang, Q. Hu, M. Wang, and J. Chao, "Applying fractal theory to characterize the pore structure of lacustrine shale from the Zhanhua depression in Bohai Bay basin, Eastern China," *Energy & Fuels*, vol. 32, no. 7, pp. 7539–7556, 2018.

[8] L. Zhang, B. Li, S. Jiang et al., "Heterogeneity characterization of the lower Silurian Longmaxi marine shale in the Pengshui area, South China," *International Journal of Coal Geology*, vol. 195, pp. 250–266, 2018.

[9] R. G. Loucks, R. M. Reed, S. C. Ruppel, and D. M. Jarvie, "Morphology, genesis, and distribution of nanometer-scale pores in siliceous mudstones of the Mississippian Barnett shale," *Journal of Sedimentary Research*, vol. 79, no. 12, pp. 848–861, 2009.

[10] M. Wei, J. Liu, D. Elsworth, and E. Wang, "Triple-porosity modelling for the simulation of multiscale flow mechanisms in shale reservoirs," *Geofluids*, vol. 2018, Article ID 6948726, 11 pages, 2018.

[11] J. B. Curtis, "Fractured shale-gas systems," *AAPG Bulletin*, vol. 86, no. 11, pp. 1921–1938, 2002.

[12] Z. Ye, D. Chen, Z. Pan, G. Zhang, Y. Xia, and X. Ding, "An improved Langmuir model for evaluating methane adsorption capacity in shale under various pressures and temperatures," *Journal of Natural Gas Science and Engineering*, vol. 31, pp. 658–680, 2016.

[13] Q. Guo, *The Research of Shale Gas Adsorption Model under High Temperature and High Pressure-Take Shale Gas Reservoir in WY Block as an Example*, Q. T. Guo, Ed., pp. 43–45, 2017.

[14] H. Han, D. H. Li, Y. Ma et al., "The origin of marine shale gas in the northeastern Sichuan basin, China: implications from chemical composition and stable carbon isotope of desorbed gas," *Acta Petrolei Sinica*, vol. 34, pp. 453–459, 2013.

[15] R. Kleinrahm, W. Duschek, and W. Wagner, "(Pressure, density, temperature) measurements in the critical region of methane," *Journal of Chemical Thermodynamics*, vol. 18, no. 12, pp. 1103–1114, 1986.

[16] D. B. Robinson, D.-Y. Peng, and H.-J. Ng, "Applications of the Peng-Robinson equation of state," in *ACS Symposium Series*, vol. 60, pp. 200–220, ACS Symposium Series, Washington, DC, USA, 1977.

[17] A. L. Lee, M. H. Gonzalez, and B. E. Eakin, "The viscosity of natural gases," *Journal of Petroleum Technology*, vol. 18, no. 8, pp. 997–1000, 1966.

[18] A. S. Ziarani and R. Aguilera, "Knudsen's permeability correction for tight porous media," *Transport in Porous Media*, vol. 91, no. 1, pp. 239–260, 2012.

[19] J. Deng, W. Zhu, and Q. Ma, "A new seepage model for shale gas reservoir and productivity analysis of fractured well," *Fuel*, vol. 124, pp. 232–240, 2014.

[20] J. Deng, W. Zhu, Q. Qi, W. Tian, and M. Yue, "Study on the steady and transient pressure characteristics of shale gas reservoirs," *Journal of Natural Gas Science and Engineering*, vol. 24, pp. 210–216, 2015.

[21] J. Liu, X. Shang, and W. Zhu, "Numerical computation for nonlinear unsteady percolation of shale gas and prediction of production," *Scientia Sinica Technologica*, vol. 45, pp. 737–746, 2015.

[22] J. Wang, H. Luo, H. Liu, F. Cao, Z. Li, and K. Sepehrnoori, "An integrative model to simulate gas transport and production coupled with gas adsorption, non-Darcy flow, surface diffusion, and stress dependence in organic-shale reservoirs," *Society of Petroleum Engineers Journal*, vol. 22, no. 1, pp. 244–264, 2017.

[23] T. Huang, Z. Tao, E. Li, Q. Lyu, and X. Guo, "Effect of permeability anisotropy on the production of multi-scale shale gas reservoirs," *Energies*, vol. 10, no. 10, p. 1549, 2017.

[24] T. Huang, E. Li, Z. Tao, and X. Guo, "A nonlinear seepage model of gas and water transport in multi-scale shale gas reservoirs based on dynamic permeability," *Journal of Geophysics & Engineering*, vol. 15, no. 4, pp. 1255–1268, 2018.

[25] X. Guo, Y. Ren, and H. Wu, "Apparent permeability model of shale gas considering stress sensitivity and adsorption," *Lithologic Reservoirs*, vol. 27, pp. 109–112, 2015.

[26] D. W. Peaceman, "Interpretation of well-block pressures in numerical reservoir simulation with nonsquare gridblocks and anisotropic permeability," *Society of Petroleum Engineers Journal*, vol. 23, no. 3, pp. 531–534, 1983.

[27] K. Wu, X. Li, C. Wang, W. Yu, and Z. Chen, "Model for surface diffusion of adsorbed gas in nanopores of shale gas reservoirs," *Industrial & Engineering Chemistry Research*, vol. 54, no. 12, pp. 3225–3236, 2015.

[28] K. Wu, Z. Chen, X. Li, C. Guo, and M. Wei, "A model for multiple transport mechanisms through nanopores of shale gas reservoirs with real gas effect–adsorption-mechanic coupling," *International Journal of Heat and Mass Transfer*, vol. 93, pp. 408–426, 2016.

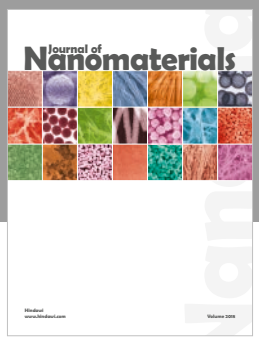

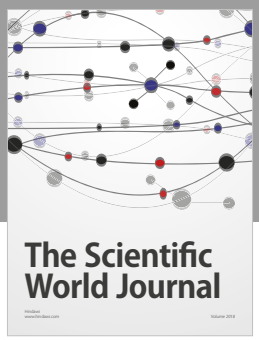

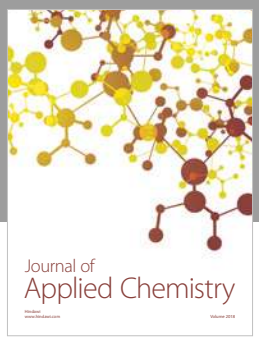

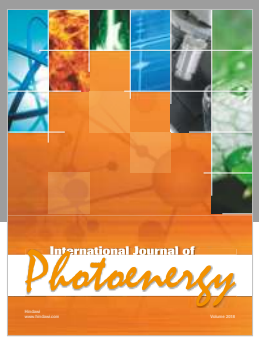

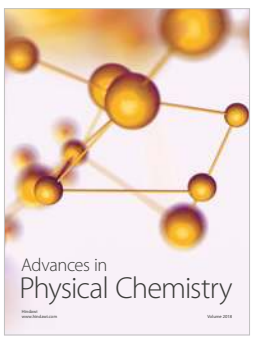

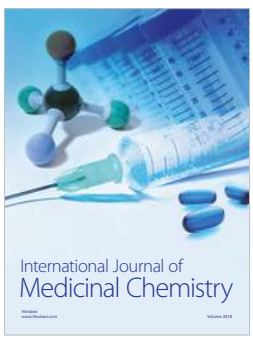

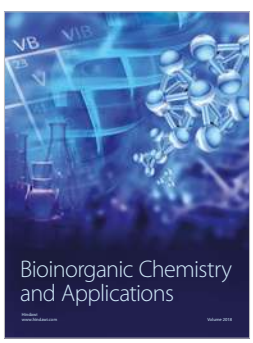

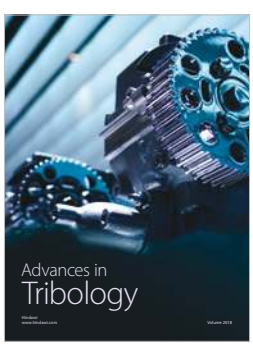

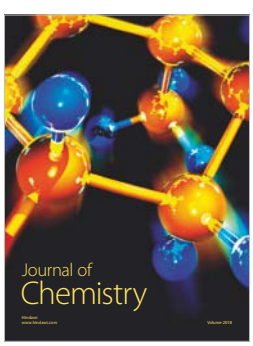

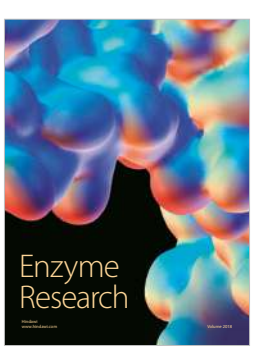

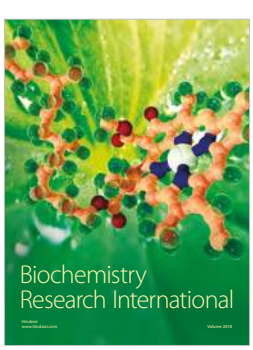


Hindawi

Submit your manuscripts at
www.hindawi.com